LUND UNIVERSITY

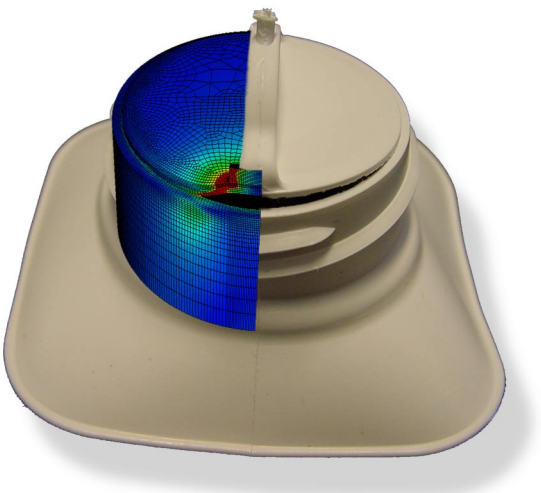

MECHANICAL BEHAVIOUR OF TEAR OPENING IN INJECTION MOULDED PLASTIC TOPS

JOHAN ISAKSSON

Structural Mechanics

Master's Dissertation

Structural Mechanics

ISRN LUTVDG/TVSM--04/5127--SE (1-55)
ISSN 0281-6679

MECHANICAL BEHAVIOUR OF TEAR OPENING IN INJECTION MOULDED PLASTIC TOPS

Master's Dissertation by

Johan Isaksson

Supervisors:

Kent Persson, Div. of Structural Mechanics

Håkan Olsson, Tetra Pak R&D AB

Printed by KFS i Lund AB, Lund, Sweden, September 2004.

For information, address:
Division of Structural Mechanics, LTH, Lund University, Box 118, SE-221 00 Lund, Sweden.
Homepage: http://www.byggmek.lth.se

Preface

This work presented in this Master's thesis was carried out at the Division of Structural Mechanics, Lund University, Sweden in cooperation with Tetra Pak R&D during March 2004 - September 2004.

I would like to express my gratitude to my supervisor Ph.D. Kent Persson at the Division of Structural Mechanics, for his guidance during this work. I would also like to thank my supervisor M.Sc. Håkan Olsson at Tetra Pak for supporting with thoughts and ideas. A special thanks to Åsa Halldén at Tetra Pak for helping me with the polymer materials as well as Tord Lundgren for the assistance during the tests performed at the Division of Structural Mechanics, Lund University.

I am also very grateful to Michael Aly, Kjell Asplund, Giorgos Papaspiropoulos at Tetra Pak and Bo Zadig at Division of Structural Mechanics, Lund University who help me with the layout.

Lund, September 2004

Johan Isaksson

Abstract

The tear opening study is conducted with an example from the Tetra Pak package industry, the Tetra Top package. The top of the package is constructed by a injection molded low density thermoplastic. The package is opened with a tear opening located on the top part.

In order to make tear opening more versatile, studies how opening forces reacts upon material modifications and alternative geometry has been made.

The vertical displacement of the *'drawstring'* (i.e. pull-bridge) concentrate the stress around the tear opening and the shallow pit (e.g. notch) located were the fracture is supposed to initiate.

The fracture initiates and the package opens when sufficient force is applied to the pull-bridge

The object of this study is how new materials affects the opening force. A alternate tougher material will in all cases increase the opening force. Modified geometry is hence, necessary to decrease the opening force.

Computational studies has shown that a alternate geometry can decrease the opening force with 56%.

Keywords: tear opening, thermoplastics, fracture mechanics, deformation softening, ABAQUS.

Contents

1. Introduction

1.1. Background

Tetra Top is an enclosable, square package with rounded corners. It has a polyethylene lid, which is injection-molded and sealed to the package in a single process. The Tetra Top package addresses consumer demand for ease of opening, pouring and enclosing. The package was introduced in 1989.[8]

Figure 1.1: *Tetra carton chilled products*

The tear opening of Tetra Pak package is constructed with a in-situ injection molded lid with a plastic part, a so-called pull-bridge. Secondly, a cap is joined with the tear opening witch makes the product re-closable after use.

The vertical displacement of the pull-bridge concentrate the stress around the tear opening and the shallow pit notch located were the fracture is supposed to initiate. The notch and pull-bridge are shown in Fig. 1.2.a & b.

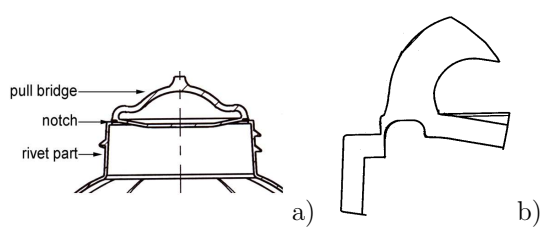

Figure 1.2: *Sketch of the tear opening, showing a) the top b) the notch and pull-bridge*

The fracture initiates and the package opens when sufficient force is applied to the pull-bridge

A alternate tougher material will in all cases increase the opening force and will make the product difficult to open. A weaker material in the top could in some cases lead the top to breakage during transportation. A tougher material could thus facilitate certain aspects of the logistics of the top.

1.2. Objective

The purpose of this study was to study and evaluate the interactions between new materials and new geometries on the opening force of the injection molded top part in the Tetra Top packages. When the material in the tear opening is changed to a tougher material the opening force increases and will in extreme cases increase the opening force to unacceptable values. In order to solve problems associated with tougher materials FE-simulations were carried out resulting in terms of opening forces and displacements at opening.

All simulations described in this report were carried out using the software ABAQUS. ABAQUS/CAE was used for creating the models and the input files, which were later modified given adequate properties. Post processing was done with ABAQUS/Viewer.

1.3. Outline

Chapter 2: Thermoplastics In this chapter an introduction to thermoplastics is given discussing their structure and mechanical properties.

Chapter 3: Constitutive models A brief review of the fracture mechanic models that will be used in the FE-modelling. The review gives an introduction to fracture zones (i.e. cohesive zones) which are essential in the construction of the FE-model.

Chapter 4: Experimental Description of the experimental tests that were conducted in order to establish material models in the FE environment and to verify the accuracy of the FE-model.

Chapter 5: FE-analysis of the tensile test FE-analysis of experimental tensile tests to determine the parameter of the material models of the studied materials.

Chapter 6: FE-modelling of tear openings FE-analysis results of the tear opening are presented which are made possible through the use of fracture mechanics, experimental tests and FE-analysis of tensile tests. Validation of the FE-model are presented using results from experimental tests of the tear opening.

Chapter 7: Numerical parameter study FE-analysis of the tear opening that were conducted with new materials and/or new geometries in order to examine its influence on the tear opening force are presented.

Chapter 8: Summary and conclusions This chapter summaries and describes the conclusions achieved in this study.

2. Thermoplastics

2.1. General remarks

In this chapter the general mechanical behavior of thermoplastics will be briefly described. For further reading about the subject see [4].

The top of the TetraTop package is made from thermoplastics of various qualities. There is, however, certain common characteristics of the mechanical behavior of thermoplastics of different quality.

Representative for plastics is large viscoelastic and plastic (viscous) deformation components. Consequently it is not possible in construction of moderate stressed plastic parts to ignore the viscoelastic effect. Polymer materials is strongly time dependent and since all tests are performed at the same strain rates the viscoelastic effect is not included in this study.

2.2. Mechanical Properties

The top is constructed of a low-density polyethylene which is a ductile thermoplastic and presents generally upon deformation three types of behaviors:

- Elastic deformation
- Viscoelastic deformation
- Plastic deformation

Stress-strain curves directly obtained from tensile measurements express the stress in force per unit area of the *original* specimen cross section, see eqn. 2.2, and the specimen cross section obviously changes continuously during the experiment and so produces a curve of type shown in Fig. 2.1.

The deformation or strain is an effect due to external forces or stresses. For small strains and uniaxial deformations, the strain, e, is conventionally represented by the change in length divided by the original length, as

$$e = \frac{l_i - l_0}{l_0} \tag{2.1}$$

Further for small strains the force, F, per original cross sectional area, A_0, gives the conventional stress, s, as

$$s = \frac{F}{A_0} \tag{2.2}$$

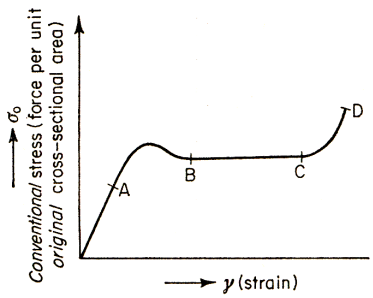

Figure 2.1: *Conventional stress-strain*

The elastic strain is the reversible part of the deformation. For thermoplastics, the initial linear part of the stress versus strain curve, shown in Fig.2.2 0-A as part from 0 to A, may often be regraded as linear elastic. The relation between stresses and strains represented by Hookes law, where E is elastic modulus.

$$s = Ee \tag{2.3}$$

The plastic behavior, indicated in Fig.2.2 as the part from A to C, is recognized by continuous deformation the yield stress, σ_y, is reached and irreversible strains without visible fractures develop.

In eqn. 2.4 elastic strain, ε^{el} and plastic strain, ε^{pl} sums up to the total strain of the material, ε_{TOTAL}.

$$\varepsilon_{TOTAL} = \varepsilon^{pl} + \varepsilon^{el} \tag{2.4}$$

For thermoplastics large strain and deformations often occur, even at moderate stress levels. Large deformations result in that nonlinear strains and changes of the original body shape develop.

Under such conditions the stresses and strains must be defined differently than in eqn. 2.2 and 2.1.

If this is done and stress in terms of force per actual cross sectional area, see eqn. 2.5, where σ indicates the Cauchy stress and ε the logarithmic strain. The stress strain is the plotted as previous curves and results in the curve shown in Fig. 2.2.

$$\sigma = \frac{F}{A} \tag{2.5}$$

Additionally the strain relations changes from the conventional strain, see eqn. 2.1, to the logarithmic strain, see eqn. 2.6.

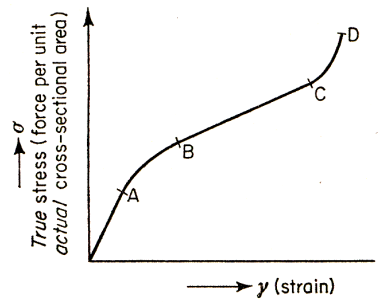

Figure 2.2: *True stress-strain*

$$d\varepsilon = \frac{dl}{l},\ \varepsilon = \int_{l_0}^{l_i} \frac{dl}{l} = ln\frac{l_i}{l_0} \tag{2.6}$$

2.3. Tensile behavior

From uniaxial tensile tests of polymer materials it can be observed that the tensile force raises with increasing strain until the yield point is reached, σ_y.

Once a ductile polymer has reached the yield point it may either deform to fracture without further increase in load, or else, it may strain harden and break under load exceeding the load at yield. Since the cross-sectional area reduces with increasing strain, the actual stress at the moment of fracture may in the latter case be considerably higher than the yield stress. The two forms of behavior, with and without strain hardening are sketched in Fig. 2.3 and may both occur in the same polymer at different temperatures or strain rates [1]. For a material which does not strain harden, the yield stress is equal the stress at fracture.

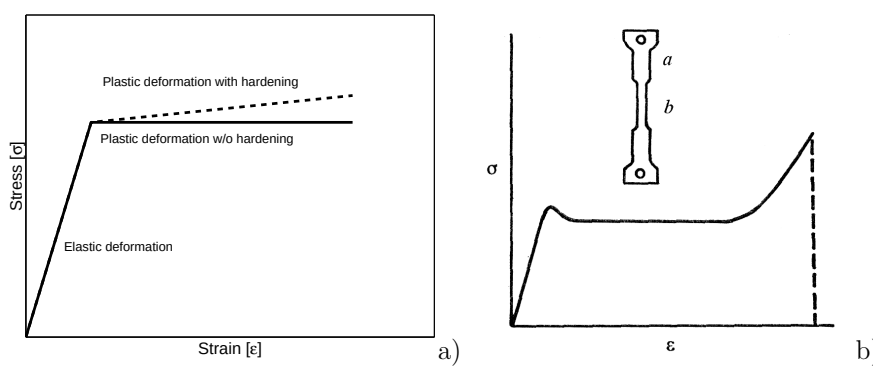

Figure 2.3: *a) Schematic descriptions of stress-strain curves with and without strain hardening, b) Stress-strain curve indicationg cold-drawing; inset is the test piece itself.*

A third behavior necking, may be observed for thermoplastics. Necking is recognized by the formation of a neck, a contraction of the cross-section, in the middle part of the tensile specimen. A typical stress-strain curve for a specimen with necking is shown in Fig. 2.3.b.

After yielding the force decreases slightly and the material can be stretched further without an increase in force. When neck formation has spread along the whole test specimen, the tensile force rises until the break point is reached (Ultimate strength, σ_F).

Additionally, further increase of stress to an already necked specimen can result in two different behaviors depending on the material properties:

- *Either* the neck becomes progressively thinner and eventually the specimen breaks
- *Or* the neck stabilize itself to a constant cross-sectional area as the shoulders travel along the specimen until they have 'consumed' all available undrawn material. This is called *cold-drawing*, shown in Fig 2.3.b.

3. Constitutive models

3.1. General remarks

The application of fracture mechanics was essential in this study. It is primarily brought into use when the tear opening is subjected to opening forces.

The initial study of the opening procedure indicated that the fracture modes changed during opening of the top where fracture in tear opening first occurred in pure opening mode, *Mode I*. The crack progressed further and the fracture mode changed to *Mode III*, tearing see Fig. 3.1.

However, since vary large strains develop prior to crack formation the material probably fracture in *Mode I* during the entire opening process as shown in Fig. 3.2.a and b.

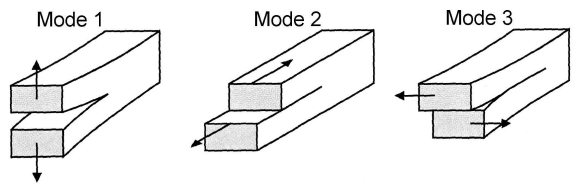

Figure 3.1: *Fracture modes*


a)
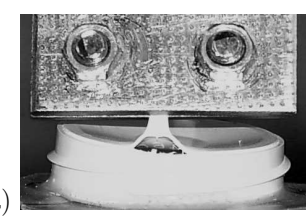
b)

Figure 3.2: *Opening procedure of the tear opening a) at opening and b) at prolonged opening*

With the initiation of the opening of the crack a cohesive zone is present, where the fracture process takes place.

Hence, the objective of this chapter is to explain the fundamentals of the cohesive zone and the introduction of the fictitious fracture model introduced by Hilleborg [7] and Barenblatt [2], in order to understand the fracture mechanics behind the opening procedure.

3.2. Material model

The material behavior of the thermoplastics is described with a material model. The behavior of the model is described by the total deformation, *or strain*, composed by the elastic and plastic strain, as

$$\varepsilon = \varepsilon^{el} + \varepsilon^{pl} \tag{3.1}$$

The material model in this case is modelled as an isotropic, linear elastic, material with no temperature dependencies.

The response of the elastic part is described, where $\mathbf{D}$ denotes the elastic stiffness matrix.

$$\sigma = \mathbf{D}^{el} \cdot \varepsilon^{el} \tag{3.2}$$

The elasticity is linear and isotropic and, can therefore, be written in terms of two material parameters. For the purpose of this development it is most appropriate to choose these parameters as the bulk modulus, K, and the shear modulus, G. These are calculated from the elastic modulus, E, and Poisson's ratio, ν as

$$K = \frac{E}{3(1-2\nu)}$$
$$G = \frac{E}{2(1+\nu)}$$

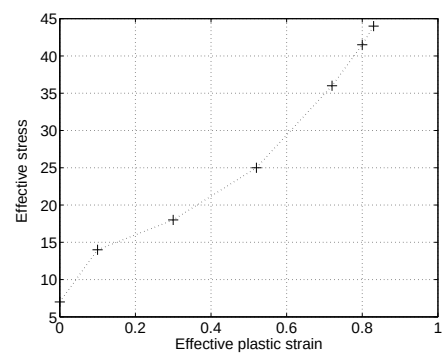

Figure 3.3: *Hardening components in effective stress-strain*

The material will be subjected to loads beyond the elastic limit and it is thus important to describe how it deforms under that load. Introducing a Mises plasticity model model with isotropic work hardening to characterize the overall response [6]. The hardening is defined as an increase in stress, allow the analysis of loading beyond the yield stress, with increasing plastic strain.

The plasticity is modelled with the effective stress, σ^{eff} and effective plastic strain, ε^{eff} following the hardening function $H(\varepsilon^{eff})$, shown in eqn. 3.3 and Fig. 3.3.

$$H(\varepsilon^{eff}) = H_0 + H'\varepsilon^{eff} \tag{3.3}$$

3.3. Introduction to cohesive zones

The fracture process is assumed to take place in a cohesive zone ahead of crack tip. In a cohesive zone, material softening is taking place, the fracture phenomenon can exhibit nonlinearity. Consider a bar of uniform cross-section subjected to monotonic extension shown in Fig. 3.4, where a sketch of the stress-elongation curve is also shown. Along the hardening portion OP of the curve the strain is uniform. At point P the tensile strength f_t is reached and linking occurs. The model assumes that a cohesive crack forms somewhere in the bar and that the bulk of the material unloads. Henceforth the bulk unloads following the curve PB while the crack concentrates the displacement as a crack opening w, which adds to the uniform strain of the bulk to give the total bar elongation (point A).

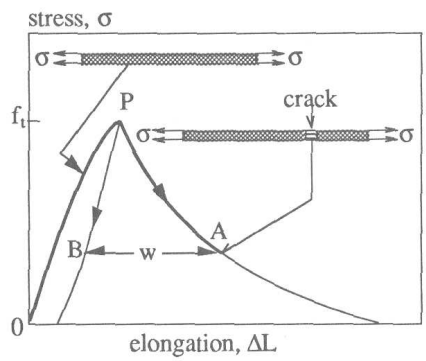

Figure 3.4: *Stress-elongation curve for a cohesive crack model*

The pre-peak response (OP) need not to be linear, but in our specific problem this point is largely irrelevant and linear elastic behavior is assumed. The specific form of the softening curve is also of little relevance and need not to be linear. The only essential features are the following: 1) it is non-negative and non-increasing, 2) for zero crack opening its values equals the tensile strength, 3) it tends to zero for large crack openings (complete failure, zero strength) and 4) it is integrable over $(0, \infty)$. This integral is the work of the fracture per unite surface of the complete crack and is denoted as G_F [3]:

$$G_F = \int_0^\infty f(w)\, dw \tag{3.4}$$

Hence, the cohesive zone is defined as the curve PBA.

3.4. Fictitious crack plane in tensile tests

The response to a uniaxial tensile test shown in Fig. 3.5.a, provides data such as elastic modulus, yield stress and ultimate strength.

Point 2 in Fig.3.5.a indicates the rupture point. The rupture seams to act instantaneous but considering a small plane which coincide with the fracture shows a softening type of behavior where the force descends with the displacement of the crack faces, u.

Consequentially, when performing experimental tensile test on the fictitious crack plane need for small clamping distance is thus necessary.

The material ahead of the fictitious crack tip is assumed to be linear, following the elastic modulus, but the material within the fracture process zone is softening; the area under the softening curve equals fracture energy G_F shown in Fig. 3.5.b.

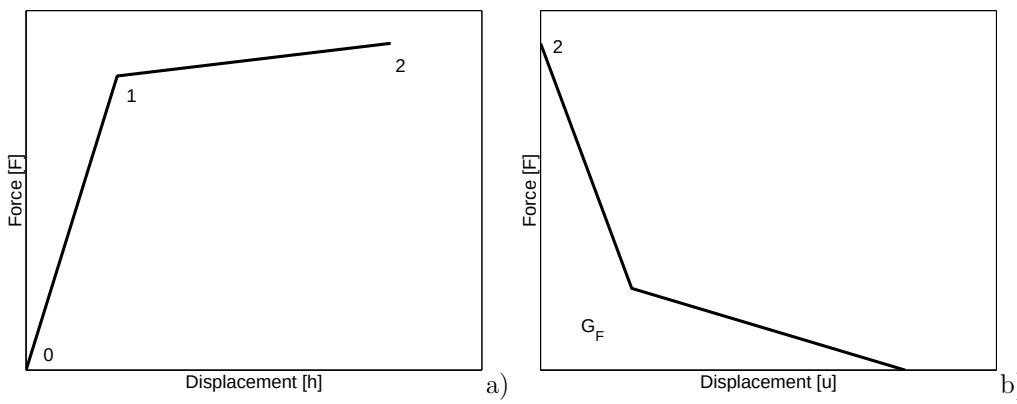

Figure 3.5: *Schematic description of the cohesive zone model*

4. Experimental

4.1. General remarks

This chapter presents the experimental tests that were made for different polymer materials in order to establish conventional material parameters such as, elastic modulus, E, elongation at break, ε_F, ultimate strength, σ_F, yield stress, σ_y, and elongation at yield, ε_y.

The tested polymer materials were the LDPE material which is currently used in the plastic tops and the BLEND and MILK materials which are proposed as new top materials.

The opening force and displacement at opening of the tear opening needs to be tested in order to verify computational results, presented later in this report. Consequently this chapter will be divided into two main parts:

- experimental tests of material specimens of different plastic materials.
- *and* experimental test of forces and deformations of the tear opening.

4.2. Tensile testing procedures

The tensile test equipment consisted generally of two clamps, which were during the experiment were displaced with increasing distance from each other. The elongation of the specimens was measured as the change in distance between the clamps. The force was measured from a load cell in the test machine. A certain amount of material flow from the clamped boundaries into the unclamped region affecting the final result. A method to minimize such effects is to perform the tensile test with a relative large clamping distance. But on the other hand capturing the deformation softening, required very small clamp distance to be applied.

Two types of test procedures for the plastic specimens were thereby established.

- To capture the deformation softening, small clamp distance was needed and the specimen required to be under deformation control.
- To establish material parameters, large clamp distance were used, due to boundaries influence on resulting stress-strain data.

4.3. Tensile testing

Roundels of three thermoplastic materials measuring $100mm$ in diameter were made. From the roundels rectangular specimens were cut measuring $80x6mm$. The material for the present tear opening, LDPE and two additional materials, BLEND and MILK material.

The rectangular specimens were mounted in the tensile testing machine as shown in Fig. 4.1 with a $25mm$ clamping distance.

Figure 4.1: *The Instron 4200 / 4300 / 4400, tensile testing machine*

The clamp were flexible and hydraulic. The lower clamp was fixed while the upper was free to move in the horizontal plane. The tests were conducted with displacement control and the upper clamp was displaced vertically, with a cross head speed of $40mm/min$. A computer connected to the machine recorded the force and the displacement of the upper clamp of a 10 samples/second.

4.3.1. Results

Fifteen specimens of the LDPE material and ten specimens of the BLEND were tensile tested. A few of the specimens broke at the clamps and a few showed different surface at break. These specimens were excluded from the diagrams and tables, resulting in nine LDPE and eight BLEND specimens tested.

As the MILK material showed large elongation at break, fewer specimens were tested because the large elongation at break made the MILK material useless as a potential top material. Seven specimens of the MILK material was thus tested and a few of them broke at the clamps and a few showed different surface at break. Resulting in a total of five MILK specimens.

The load - displacement curves for the LDPE and the BLEND materials, shown in Fig. 4.2 reveal certain strain-hardening after the yield point. For those two materials, neck-formation according to the first case scenario presented in section 2.3, where the neck becomes progressively thinner and eventually a crack forms and the specimen breaks.

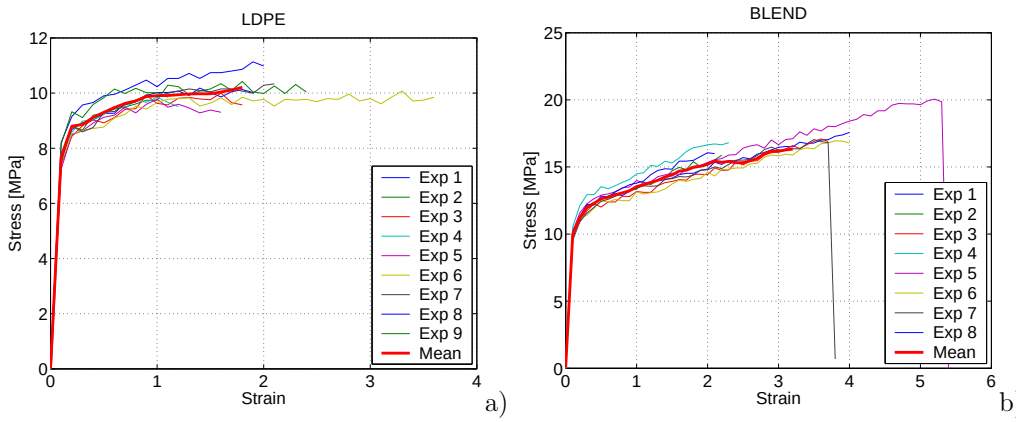

Figure 4.2: *Tensile test results for the a) LDPE material and the b) BLEND material*

The MILK material revealed a certain small amount of strain softening after yield as shown in Fig. 4.3. For this material, neck-formation according to the second case scenario, in section 2.3 was found. In this case the neck stabilize itself to a constant cross-sectional area as the shoulders travel along the specimen until they have 'consumed' all available undrawn material, known as *cold-drawing*.

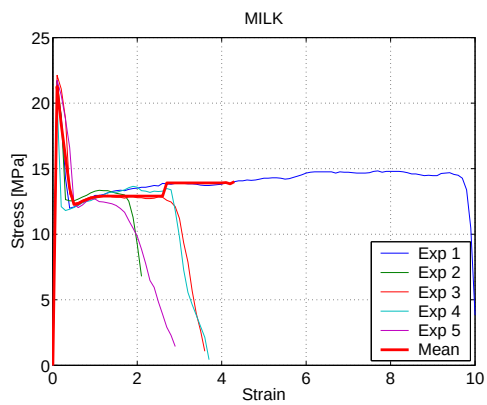

Figure 4.3: *Tensile test results for the MILK material*

The MILK material showed large elongation before break, as shown in Fig. 4.4, and will with use in the top contribute to an increase in displacement at opening. A large displacement at opening will also activate a larger surface in the cohesive zone and the tear opening force will thus increase to unacceptable values.

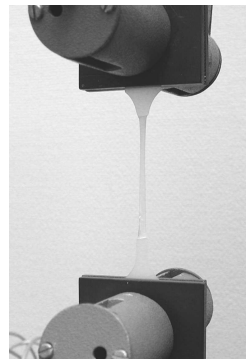

Figure 4.4: *Tensile testing of the MILK material*

Hence, the MILK material will not be considered as a potential material for the top.

The results form the tensile tests presented in table 4.1 are in conventional stress strain measures and not expressed as true stress and strain.

The tensile tests for the three materials showed great variability in terms of elongation at break whereas the ultimate strength, elongation at yield, yield stress and break strength showed much less variability.

Parameter	*a)* **LDPE**	*b)* **BLEND**	*c)* **MILK**
Elastic modulus, E	$174MPa$	$268MPa$	$870MPa$
Elongation at break, ε_F	1.82	3.2	4.35
Ultimate strength, σ_F	$10.5MPa$	$16.3MPa$	$3.38MPa$
Elongation at yield, ε_y	0.12	0.14	0.10
Yield stress, σ_y	$8.2MPa$	$10.8MPa$	$21.47MPa$

Table 4.1: *Mean values from the tensile tests*

4.4. Deformation softening testing

In order to capture the deformation softening for a plastic material, the gauge length needs to be very small and the tensile test machine must be very stiff since the amount of elastic energy must be kept at minimum in the test setup to ensure stable fracture development testing.

A certain amount of material flow from the material at the clamps will in this experiment affect the results more than in previous experiments. The objective of these experimental tests was to measure the force and displacement during the deformation softening in the cohesive zone.

A hydraulically driven MTS (Material Test System) machine was used for testing the specimens and to capture the deformation softening. The machine can be controlled either by force or displacement as function of time. This is made by a computer connected to the MTS, controlling the upper hydraulic piston which consequentially controls the upper clamp. The load cell was mounted on the upper piston, recording the force as a direct result of the stress in the test specimen. The lower piston was fixed in translation or rotation.

Data in terms of relative displacement and force were recorded at 100 samples/sec during testing, giving the information needed for evaluation and determination of the deformation softening of the material.

Before loading, the specimen was thoroughly mounted in the MTS in order not damage the specimen.

The size of the specimens measured 5x0.7mm and was mounted with a clamp distance of 0 to 1mm, as shown in Fig. 4.5.

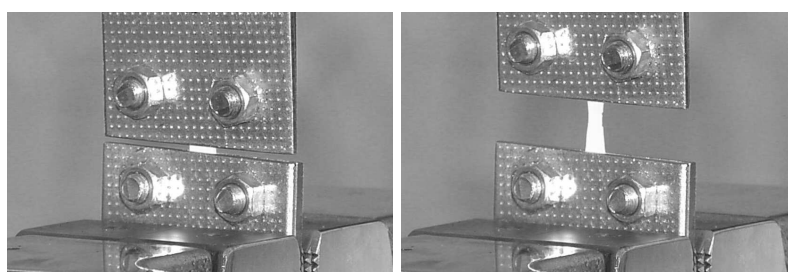

Figure 4.5: *Deformation softening testing*

4.4.1. Results

It is however not easy to capture the deformation softening for the LDPE material. Five specimens were tested but only one made it possible to capture the softening behavior.

The tests were performed only for the LDPE material. All specimens were tested under displacement control.

The oscillating values shown in the diagrams comes from the load cell being to insensitive for the small forces that developed.

In Fig. 4.6.a the complete force-displacement curve is shown whereas in Fig. 4.6.b only the deformation softening part is shown. Hence, the softening behavior of the cohesive zone is shown.

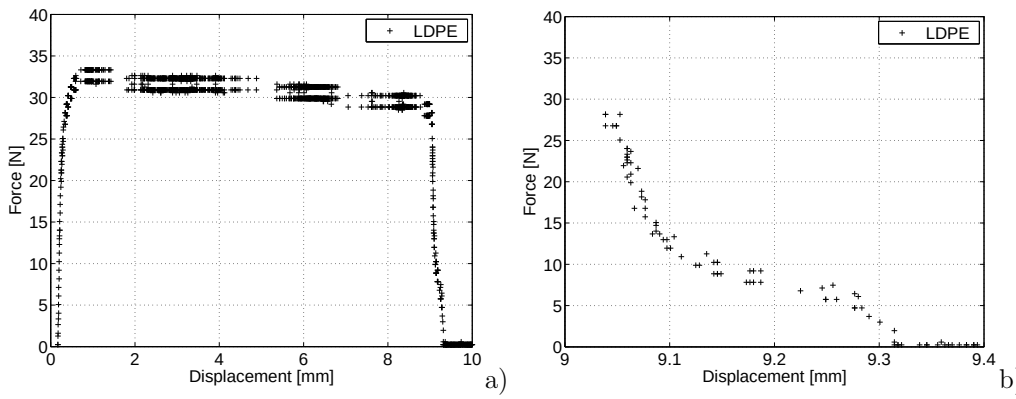

Figure 4.6: *a) The compleat tensile test curve for the LDPE material and the b) deformation softening at fracture*

4.5. Tear opening performance

In order to verify the accuracy of the computational model, the forces and displacement that arise when opening the tear opening was required to be tested.

Tops from the LDPE material was provided by Tetra Pak from which specimens were cut out. The top was constrained by casting the lower part of the top in a two component epoxy glue as shown in Fig. 4.7.a, a bolt was casted to the top since the clamps need something to grip on to. This arrangement prevented the tear opening from rotational and translative movements. The rigid constraining of the lower part of the top was needed in order to obtain accurate data.

A hydraulic driven tensile test machine (Instron 4200/4300/4400) with load cells and flexible hydraulic clamps was used in the testing. The lower clamp was fixed while the upper clamp was allowed to translate in the $\mathbf{z^{(1)}}$ and $\mathbf{x^{(1)}}$ direction as shown in Fig. 4.7.b. The tests were conducted with displacement control where the upper clamp was translated in the $\mathbf{y^{(1)}}$ direction with a cross head speed of $40mm/min$.

A computer connected to the machine recorded load and the displacement of the upper clamp with 10 samples/sec.

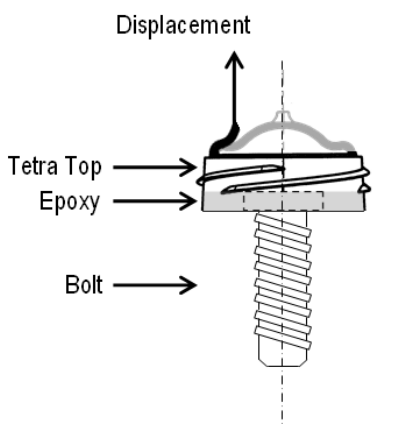

a)

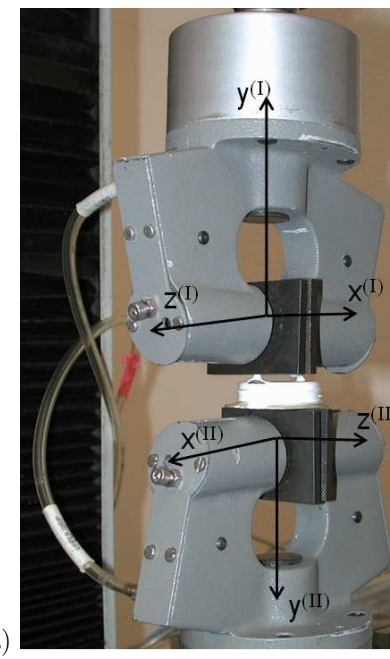

b)

Figure 4.7: *Specimen setup for tear opening tests*

4.5.1. Results

Data in terms of relative displacement and force were recorded and plotted in load-displacement diagrams shown in Fig. 4.8. Four different test were performed for the LDPE tops and a mean curve was calculated from the experimental results represented by the solid line in Fig. 4.8.

Points represented in the plot are, the maximal tear opening force, F_{op} and the relative displacement at maximal force, u_{op}.

The average tear opening force was calculated at $26.6N$ and the opening displacement at of $1.35mm$.

The Fig. 4.9.a. shows the displacement of the pull-bridge u, where u is greater than u_{op}. At u_{op} the whole surface under the pull-bridge breaks at once. Thus the maximal force of the tear opening namely the opening force. Prolonged opening decrease the tear opening surface as shown in Fig. 4.9.b. and the force decreases.

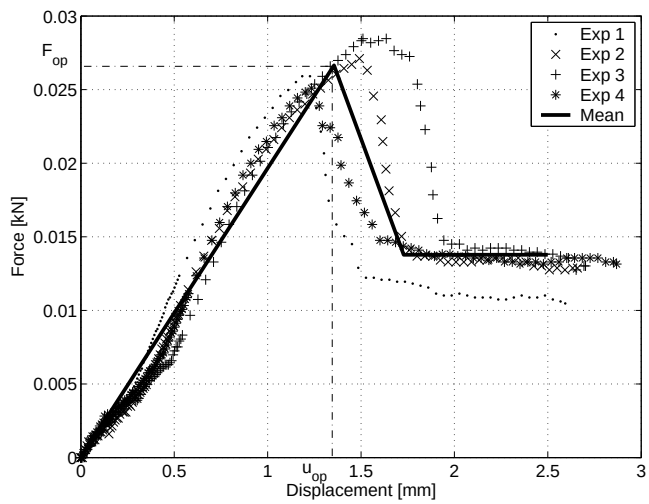

Figure 4.8: *Experimental tear opening tests*

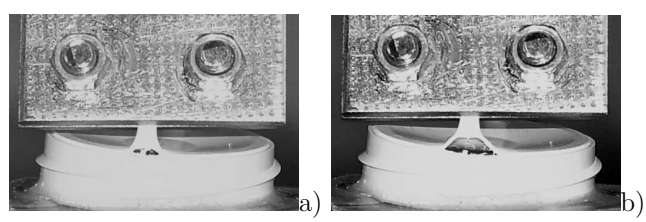

Figure 4.9: *Opening procedure of the tear opening a) at u_{op} b) at $u > u_{op}$*

4.6. Concluding remarks

The results from the tensile tests showed great variability in elongation at break but less variability in elastic modulus, yield stress, elongation at yield and ultimate strength. Mean values were established from the tensile test results as shown in table 4.2.

The MILK material showed strain hardening and large deformations and will therefore not be a suitable candidate for replacing the current material. It will therefor not be considered in further analysis. Tensile test data from the BLEND and LDPE material will, however, be used in chapter 5 and 6.

Material quality	E	ε_F
LDPE	$174MPa$	1.82
BLEND	$268MPa$	3.2
MILK	$870MPa$	4.35

Table 4.2: *Experimental results of the tensile tests*

Material quality	F_{op}	u_{op}
LDPE	$26.6N$	$1.35mm$

Table 4.3: *Experimental results for the tear opening test*

Experiments of the tear opening with the LDPE material were tested and presented data as shown in table 4.3.

Displacement controlled tensile testing with high accuracy was required to determine the softening curve of the LDPE material.

5. FE-analysis of tensile test

5.1. General remarks

In this chapter the procedures to assign the experimentally determined parameters to the material model are described. In chapter 3 it was concluded that the material model have to be expressed in true stress-strain in order to achieve accurate results from the FE-analysis of the tensile tests. The true stress-strain curve depends on the actual cross sectional area instead of the initial cross sectional area as in the conventional stress-strain.

The test setup that was used in the experimental tensile tests was simulated in the FE-environment where specimens of a certain length was subjected to loads. The goal of the FE-simulations of the tensile test was that the FE-analysis provided similar force-relative displacement curves as to the results obtained from tensile test experiments.

The material data which governed the load-displacement in the FE-simulations was altered until an exact fit with the experimental curves was achieved.

The final FE-simulations provided thus with the material parameters in form of true stress strain.

5.2. FE-model

A FE-model of the plastic experimental specimen was created in ABAQUS/CAE. The clamps were modelled by applying boundary conditions to each end. The model was thus measuring 10x5x0.7mm. The upper boundary was translated vertically with 2-3.5mm. The lower boundary was fixed. In Fig. 5.1 the model is shown.

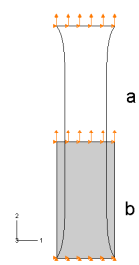

Figure 5.1: *Tensile test of a) the deformed and b) the undeformed specimen*

Since the model was thin and all loading were applied in the plane, a 2 dimensional model was created assuming plane stress conditions. The 2-D model represented the true conditions sufficiently well and reduced the CPU-time needed compared to a full 3-D model.

The element type used in the simulation was the plane stress two-dimensional ABAQUS element CPS4R which is a 4-node bilinear element with reduced integration and hourglass control.[5]

5.3. Results

The curves obtained in the experimental tensile tests of the LDPE and BLEND material were fitted with the curves obtained in the FE-simulation of the tensile tests, described earlier.

These two load-displacement curves coincide as shown in the Fig. 5.2.a, where the curve denoted *mean* is the result from the experimental tensile tests and the curve denoted *FE1* is the load-displacement curve from the FE-analysis of the tensile tests. The true stress strain relation of the LDPE material is thus encountered as shown in Fig. 5.2.b where the *FE1* curve is the true stress-strain curve of the LDPE material.

The *FE 2* curve in Fig. 5.2.a was fitted to the experimental results of the tensile test of the LDPE material but with prolonged elongation at break.

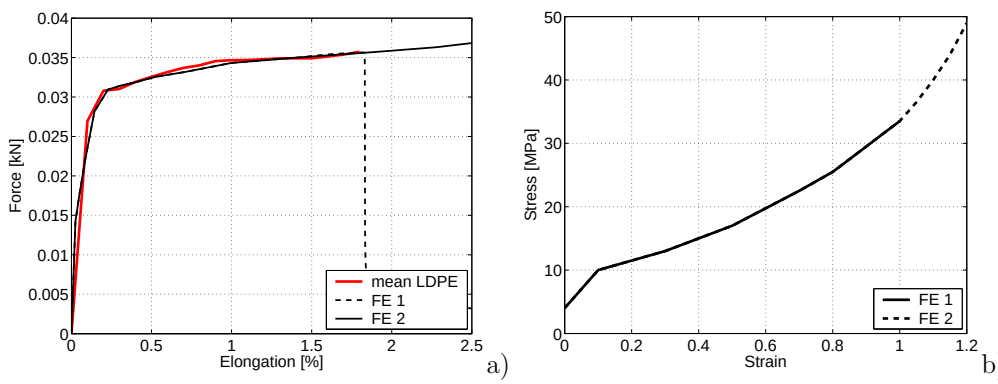

Figure 5.2: *The results from the FE-analysis of tensile test where the a) load-displacement curves of the FE-analysis and the experimental test curve are superposed and the b) true stress-strain relation of the LDPE material in the FE-analysis of tensile tests.*

The BLEND material was experimentally tested in chapter 4 and resulted in the curve denoted *mean* as shown in Fig. 5.3.a. This *mean* curve was fitted with a curve from the FE-analysis of the tensile test, denoted *FE1* as shown in Fig. 5.3. The true stress strain relation of the BLEND material is thus encountered as shown in Fig. 5.3.b where the *FE1* curve is the true stress-strain curve of the BLEND material.

The *FE 2* curve in Fig. 5.3.a was fitted to the experimental results of the tensile test of the BLEND material but with prolonged elongation at break and correspond at the curve denoted *FE2* in Fig 5.3.b.

The material parameters of the BLEND and LDPE material expressed in true stress and strain are thus shown in Fig. 5.2.b and 5.3.b.

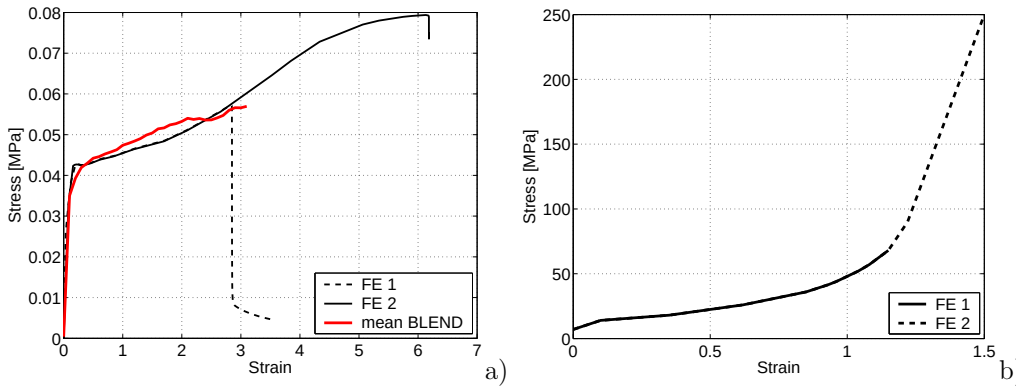

Figure 5.3: *The results from the FE-analysis of tensile test where the a) load-displacement curves of the FE-analysis and the experimental test curve are superposed and the b) true stress-strain relation of the BLEND material in the FE-analysis of tensile tests.*

6. FE-modelling of tear opening

6.1. General remarks

This chapter describes the FE-model of the tear opening and its performance during the opening procedure. The material parameters of the FE-model will be based on the experimental results presented in chapter 4 and on the fitting procedure from the FE-analysis of tensile tests presented in chapter 5.

The goal of the modelling of tear opening was not to construct a model that achieved results that produced exact responses as the experimental tests of the tear opening, but that produce qualitatively good results that could give the direction of geometrical and material changes.

The computational model is therefore constructed with approximations to the geometry of the top and material resulting in less CPU-usage and geometry that may be easily changeable.

6.2. FE-model

The geometry of the top was built with reference to the actual Tetra Top. In Fig. 6.2 the FE-model and the actual Tetra Top is shown.

On the top or the lid, a drawstring, i.e. pull-bridge is located, as shown in Fig. 6.1.a. The pull-bridge is constructed with a smooth geometry but in order to facilitate easier meshing and minimize CPU-time, the modelling of the pull-bridge were not modelled exactly as the actual pull-bridge. In Fig. 6.2.a and b the FE-model and the top is shown, where the geometry of the top is compared with the geometry of the FE-model.

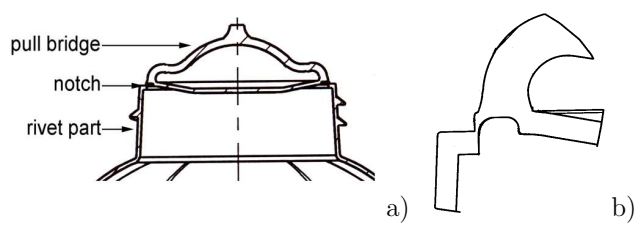

Figure 6.1: *Sketch of the tear opening, showing a) the top and b) the notch and a part of the pull-bridge*

The model was built with the aim of analyzing the opening procedure of the tear opening. The procedure was simulated by applying an opening force to the pull-bridge.

The model was built with the real geometry as reference but in order to minimize CPU time the symmetry of the problem was utilized and only half the tear opening was modelled.

Certain approximations has been made in order to simplify the modelling and to reduce the CPU-usage. A more simple intersection point between the pull-bridge and the lid, shown in Fig. 6.2.a, was modelled. The notch was also absent in the analysis. However, the approximations that were made produced results of the FE-model that was qualitatively those of the actual tear opening.

The dimensions and form of the FE-model with approximations of pull-bridge and notch is shown in Fig. 6.3.

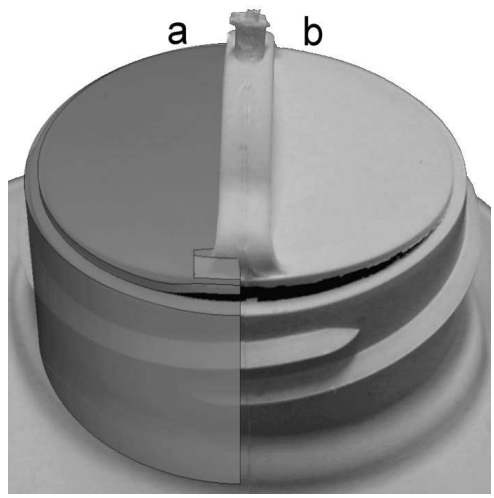

Figure 6.2: *a) the FE-model superposed on the b) tear-opening part*

To simulate the behavior of the tear opening when subjected to opening force, boundary conditions are essential for making the simulations similar to the true behavior of the tear opening. The bottom of the model was encastered. The displacement of the upper surface of the pull-bridge was prescribed to a reference node. The reference node was translated vertically until failure.

The model was divided into several sections in order to have full control of the meshing techniques. The mesh was made more dense near the pull-bridge and to minimize CPU-time the part of the mesh, where only small deformations encountered, where made more coarse.

The element type was C3D8R which is a 8-node linear brick with reduced integration element and hourglass control. Where reduced-integration elements use one fewer integration point in each direction than the fully integrated elements.

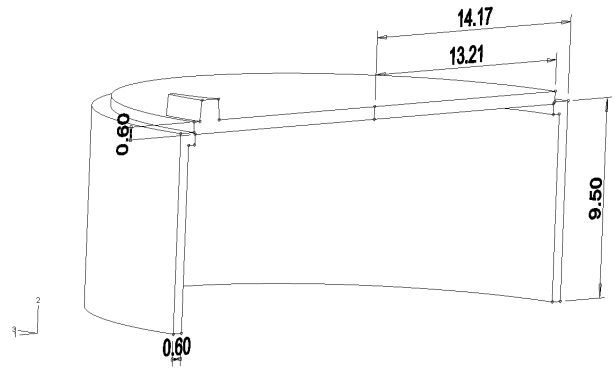

Figure 6.3: *Dimensions [mm] of the FE-model of the top*

Reduced-integration, linear elements have just a single integration point located at the element's centroid. Linear reduced-integration elements may lead to that zero energy modes develop, called hourglassing. In ABAQUS a small amount of artificial "hourglass stiffness" is introduced in reduced-integration elements to limit the propagation of hourglass modes. This stiffness is more effective at limiting the hourglass modes when more elements are used in the model, which means that linear reduced-integration elements can give good results as long as a reasonably fine mesh is used [5].

6.3. Fictitious crack plane

A fictitious crack plane is introduced in the intersection between the lid and the rivet parts because the crack initiation and propagation always occurs in this intersection. The fictitious crack plane provides the FE-model with fracture mechanic features where the behavior of the plane is realized by adding non-linear springs. In Fig. 6.4 the properties of the springs are shown in a force-relative displacement diagram where the figures a., b., and c. correspond at the tensile test specimen at $F < F_1$, $F \leq F_1$ and $F \geq F_1$, respectively.

Force is applied to the pull-bridge leading the springs to extend with a certain stiffness until F_1 is reached, showed in Fig. 6.4. Once the springs has reach a certain point, the force descends in a softening manner, simulating the fracture of the model.

The initial slope of the springs force-relative displacement is governed by the elastic modulus and the F_1 value by the ultimate strength of the material as determined in the experimental tests and on the influencing element area of the node connected to the springs.

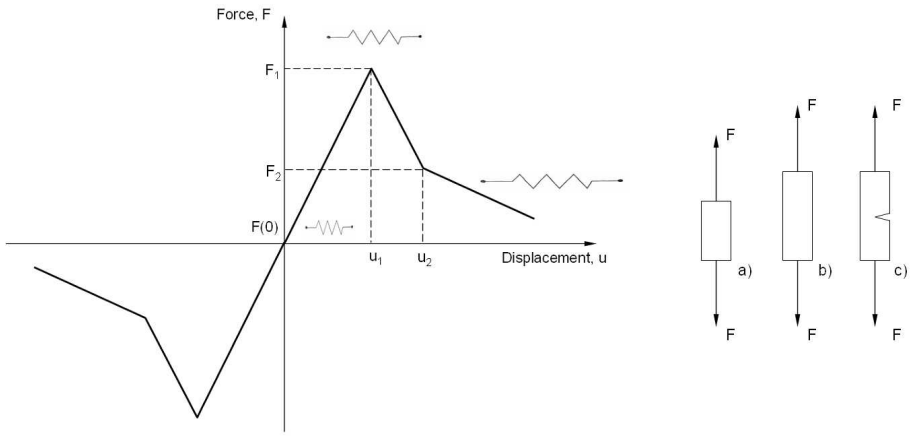

Figure 6.4: *Schematic description of the behavior of the springs in the fictitious crack plane*

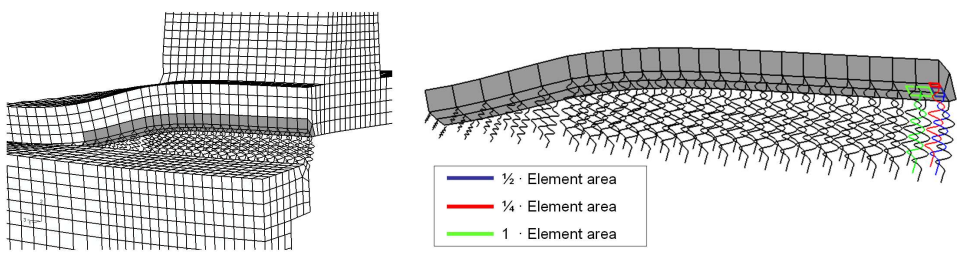

Figure 6.5: *The fictitious crack plane in the FE model.*

For the LDPE material, the ultimate strength was determined by the experimental tests in chapter 4 and by the FE-analysis in chapter 5 to $33.5MPa$. F_1 may be determined as

$$F_1[N] = \frac{\sigma_F}{A_{el}} \tag{6.1}$$

where σ_F is the ultimate strength and A_{el} is the spring's influencing area, shown in Fig. 6.5. The displacement u_1 is given by

$$u_1[mm] = \frac{F_1}{A_{el} \cdot E} \tag{6.2}$$

where E is the elastic modulus.

The prolongation of the curve that describes the behavior of the springs is described by the fraction of the maximal force, F_1, and is one third of F_1. The displacement, u_2, is 0.4.

As indicated in Fig. 6.5 there are three different influencing areas to the springs, A_{el}, $\frac{A_{el}}{2}$ and $\frac{A_{el}}{4}$. Introducing these areas into eqn. 6.1 and 6.2 the spring properties for the LDPE material can be determined as shown in table 6.1.

$u_i\ [mm]$	$1 \cdot F_i\ [N]$	$\frac{1}{2} \cdot F_i\ [N]$	$\frac{1}{4} \cdot F_i\ [N]$
-1	0	0	0
-0.4	-0.11	-0.056	-0.028
-0.19	-0.33	-0.17	-0.084
0.19	0.33	0.17	0.084
0.4	0.11	0.056	0.028
1	0	0	0

Table 6.1: *Spring properties calculated for the LDPE material*

The load-displacement curves in true stress-strain relations achieved in chapter 5 for the LDPE and the BLEND material are shown in Fig. 6.6.a and b. The spring behavior is described by the maximal stress of the $FE1$ curve by the use of eqn. 6.1-6.2 resulting in values shown in table 6.1. While the FE-model is assigned the behavior shown in Fig. 6.6.a $FE2$, leading the springs to failure before the solid.

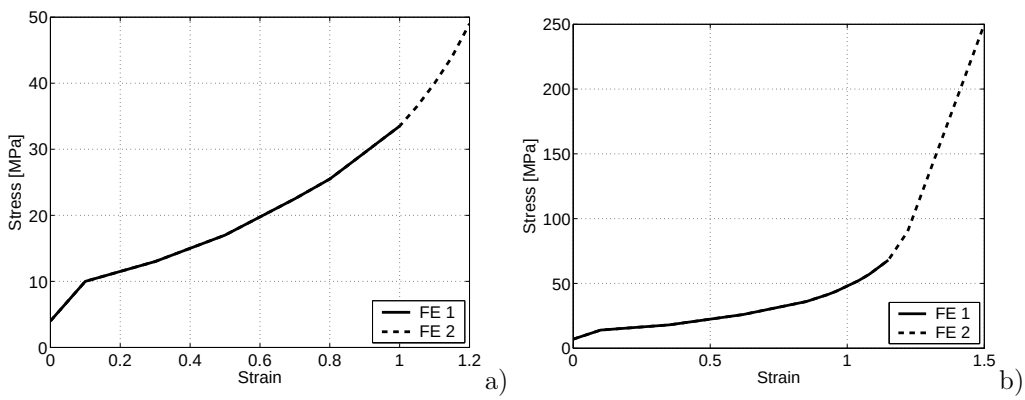

Figure 6.6: *True stress-strain relations for the a) LDPE material and b) the BLEND material*

6.4. Results

The results of the simulations presented in this section aim at showing the accuracy of the FE-model of the injection molded tear opening.

Fig. 6.7 shows the results of the FE-model, denoted FE, in comparison to the experimental data of the opening forces of the injection molded part denoted $Mean$. The absence of the notch in the FE-model gives deviant behavior compared to the experimental tests of the tear opening.

Further studies and experience from the tear opening has shown that the notch can contribute with a ∼10% decrease of the opening force. Thus, the curve labelled *Mean sim. w/o notch* shows a calculated version of the tear opening without the notch.

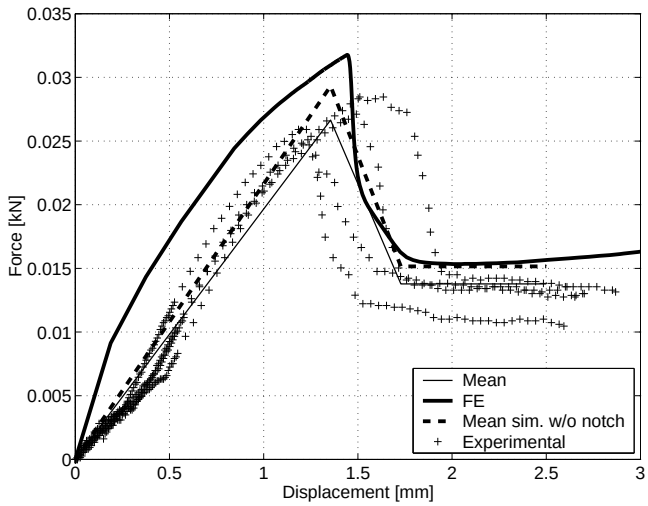

Figure 6.7: *Load-Displacement diagrams for the opening of the FE-model with the LDPE material compared with the experimental results of the tear opening*

The material in the FE-model was changed to a more tougher material, previously tested as the BLEND material in chapter 4. Consequently the tear opening force increase and would be harder to open. In Fig. 6.8 the results from the FE-analysis of the BLEND material is shown. The tear opening force, F_{op}, equals 63.4N, a nearly ∼100% increase as compared with the LDPE material.

Since no experimental tests has been made for the tear opening with the BLEND material, the accuracy of the FE-model with the BLEND material can not be verified.

However, since the FE-model with the LDPE material verifies the FE-model sufficiently well and assumptions can be made that the FE-model with the BLEND material is accurate and presents qualitative results.

The only curve showed in the figure is thus the one from the FE-analysis of the tear opening with the BLEND material.

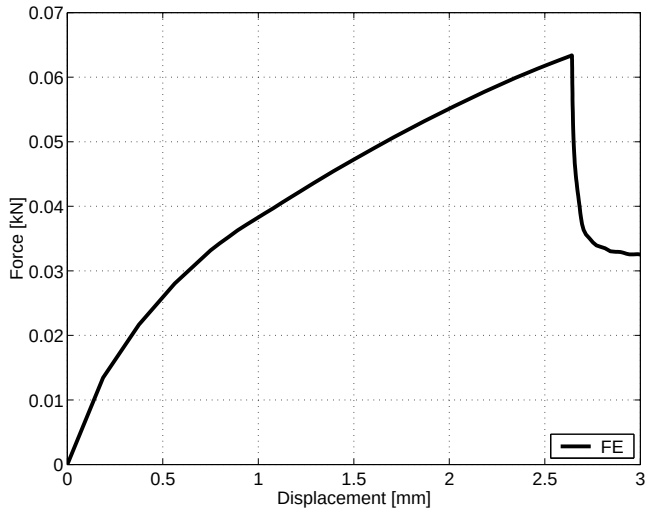

Figure 6.8: *Load-Displacement diagrams for the opening of the FE-model with the BLEND material*

Table 6.2 shows the values corresponding at the curves presented earlier. The presented values are the opening force, F_{op}, and the displacement at opening, u_{op}.

Plot	F_{op}	u_{op}
LDPE		
Mean(Experimental)	$26.6N$	$1.36mm$
FE	$31.5N$	$1.42mm$
Mean(Experimental) sim. w/o notch	$29.3N$	$1.36mm$
BLEND		
FE	$63.4N$	$2.64mm$

Table 6.2: *Results of the FE-model with LDPE & BLEND materials compared with the experimental results*

7. Numerical parameter study

7.1. General

In this chapter, a parameter study made in order to establish relationships between material, package design and tear opening force is presented.

Parameters that will be studied are ultimate strength, σ_F, yield stress, σ_y, elastic modulus, E, and fracture energy, G_F.

The FE-model described in chapter 6 was in this study a slightly weaker material than the described LDPE material.

The approach of this study was to vary one material parameter at the time from a reference material. The material parameters of the reference material is shown in table 7.1.

Material data, LDPE	**Values**
Elastic modulus, E	$134MPa$
Poisson's ratio, ν	0.34
Ultimate strength, σ_F	$9.37MPa$
Yield stress, σ_y	$7.85MPa$
Elongation at break, ε_F	0.56
Elongation at yield, ε_y	0.05

Table 7.1: *Material properties for the reference material (True stress-strain)*

Using eqn. 6.1 and eqn. 6.2 the spring properties for the reference material were determined as shown in Table 7.2.

As a result of the parameter study, opening forces will be presented with the change of material parameter and package design, where opening forces are described as the maximal force in the load-displacement diagrams.

Additionally, the development of stress concentrations in the fictitious crack plane was studied as shown in Fig. 7.1.b where the bold curve indicates the highest stress concentration.

Each curve in the diagram represents one node in the fictitious crack plane as shown in Fig. 7.1.a where the node with the highest stress concentration is marked with a larger dot.

$u_i\ [mm]$	$1 \cdot F_i\ [N]$	$\frac{1}{2} \cdot F_i\ [N]$	$\frac{1}{4} \cdot F_i\ [N]$
-1	0	0	0
-0,4	-0,032	-0,016	-0,008
-0,069	-0,095	-0,047	-0,024
0,069	0,095	0,047	0,024
0,4	0,032	0,016	0,008
1	0	0	0

Table 7.2: *Spring properties for the reference material*

The highest stress concentration where the opening initiate is preferentially close to the symmetry plane which will decrease the opening force.

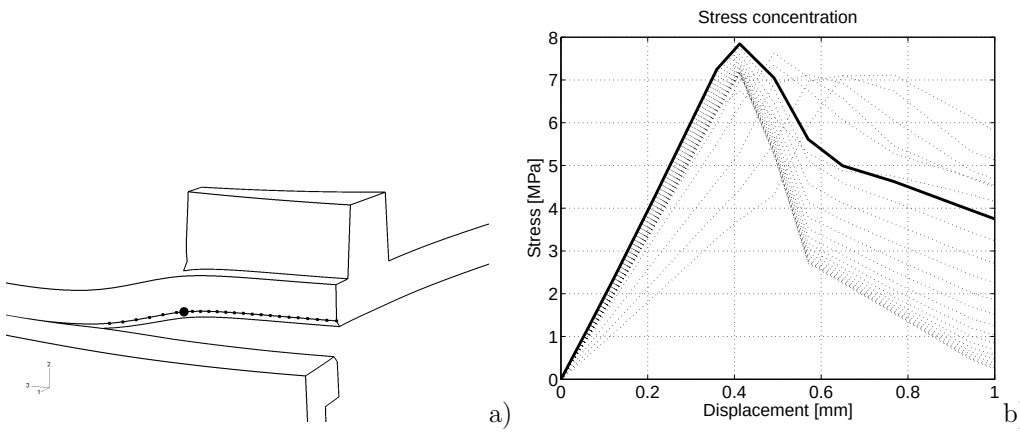

Figure 7.1: *a) The nodes in the fictitious crack plane and b) the stress concentration curves for each node in the reference material*

7.2. Material parameters

The influence of the material in the plastic top on the tear opening force was studied by modifying the material. The material was modified by varying material parameters such as the elastic modulus, yield stress, ultimate strength and the fracture energy. The range of the material parameters that were varied is shown in table 7.3.

Parameter	**Range**
Elastic modulus, E	100-500MPa
Yield stress, σ_y	5.38-7.85MPa
Ultimate strength, σ_F	9.37-13.98MPa
Fracture energy, G_F	$2.13 \cdot 10^3 - 3.33 \cdot 10^3 N/m$

Table 7.3: *Parameter range*

Elastic modulus

An increase of the elastic modulus makes the FE-model more stiffer and the initial slope in the spring's properties more steep. Hence,

$$E_{ref} < E \tag{7.1}$$

where E_{ref} and E is the elastic modulus of the reference material and of the new material, respectively. Modification of the initial slope of the spring behavior will either alter the maximal strength of the springs, F_1 or the elongation of the springs at maximal strength, u_1.

Since the maximal force of the springs, analog with the ultimate strength, is a variable in this parameter study, the elongation of the springs at maximal strength will be changed accordingly:

$$u_1(E_{ref}) > u_1(E) \tag{7.2}$$

Yield stress

An increase in yield stress will increase the elastic part of the material and will not affect the properties of the springs.

Ultimate strength

Increasing the ultimate strength makes the material tougher and will affect the maximal strength, F_1, of the springs.

$$\sigma_{F_{ref}} < \sigma_F \tag{7.3}$$

$$F_1(\sigma_{F_{ref}}) < F_1(\sigma_F) \tag{7.4}$$

Fracture energy

The fracture energy is defined as the area under the curve $F(u)|_{u>u_1}$ as shown in Fig. 6.4.

In the parameter study three values of fracture energy, G_F are studied, $3.33 \cdot 10^3 N/m$ for the reference material, $2.96 \cdot 10^3 N/m$ and $2.13 \cdot 10^3 N/m$. The points F_2 and u_2 were defined as shown in table

G_F $[N/m] \cdot 10^3$	F_i $[N]$	u_i $[mm]$
3.33	$F_2 = \frac{F_1}{3}$	$u_2 = 0.4$
	$F_3 = 0$	$u_3 = 0$
2.96	$F_2 = \frac{F_1}{4}$	$u_2 = 0.4$
	$F_3 = 0$	$u_3 = 0$
2.13	$F_2 = \frac{F_1}{6}$	$u_2 = 0.3$
	$F_3 = 0$	$u_3 = 0$

Table 7.4: *The G_F values in the parameter study*

7.3. Design parameters

The package design influence on the tear opening force was studied by modifying the notch and / or the pull-bridge.

Three different cases of the notch were studied, the first case was the reference model which had an absence of the notch, the second case which were similar to the top and a third case was the length of the notch was extended.

Two different cases of the pull-bridge were studied.

Pull-bridge

The study of the pull-bridge was based on the position and not on the geometrical form of the pull-bridge.

The positions that were studied was the standard position, as in the top, as shown in Fig. 7.2.a and an alternate positions where the pull-bridge was rotated 90° and also moved to the edge of the lid as shown in Fig. 7.2.b

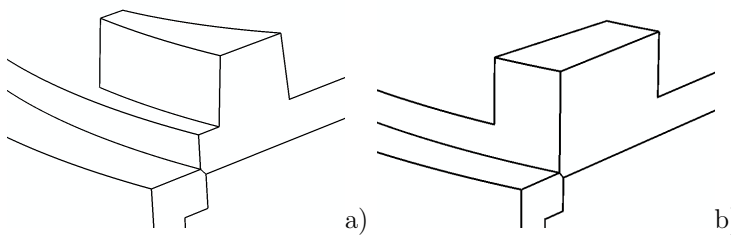

Figure 7.2: *a) The standard position as in the top and b) the alternate position of the pull-bridge*

Notch

The FE-model were assigned two different sizes of notches as described earlier. The notch in the top is described by a decrease of the cross-sectional area of the section where the fracture initiate. A decrease of the cross sectional area in the FE-model is however simulated by a decrease of the spring's influencing area, introduced in chapter 6. The notch in the FE-model is thus simulated by modifications of the non-linear springs.

The sizes of the notches are presented in table 7.5 where r represent the ratio between the length of the pull-bridge and the notch, shown in eqn. 7.5. The notch in the top presented a ratio of 0.304 compared with the simulated notch in the FE-model that presented a ration of 0.444. The simulated notch in the FE-model is hence slightly larger than the notch in the top.

$$r = \frac{l_{notch}}{l_{pull-bridge}} \tag{7.5}$$

An increase of the elastic modulus makes the FE-model more stiffer and the tear opening force increases. The results of the parameter study shown in diagram 7.3.a indicates that the initial slope increases and that the zone around the tear opening force, F_{op}, is more rounded. Additionally, the force after the tear opening force descends more rapidly with low values of elastic modulus.

The most important response of the parameter study is the ultimate strength, σ_F, where an increase describes a significant increase of the maximal tear opening force, F_{op}, as shown in diagram 7.3.b.

The modification of the yield stress parameter shows no significant change in the tear opening force as shown in diagram 7.3.c.

The modification of the fracture energy parameter shown in diagram 7.3.d shows to have no influence on the tear opening force, F_{op}. However, the force after the tear opening force descends more rapidly with low values of fracture energy.

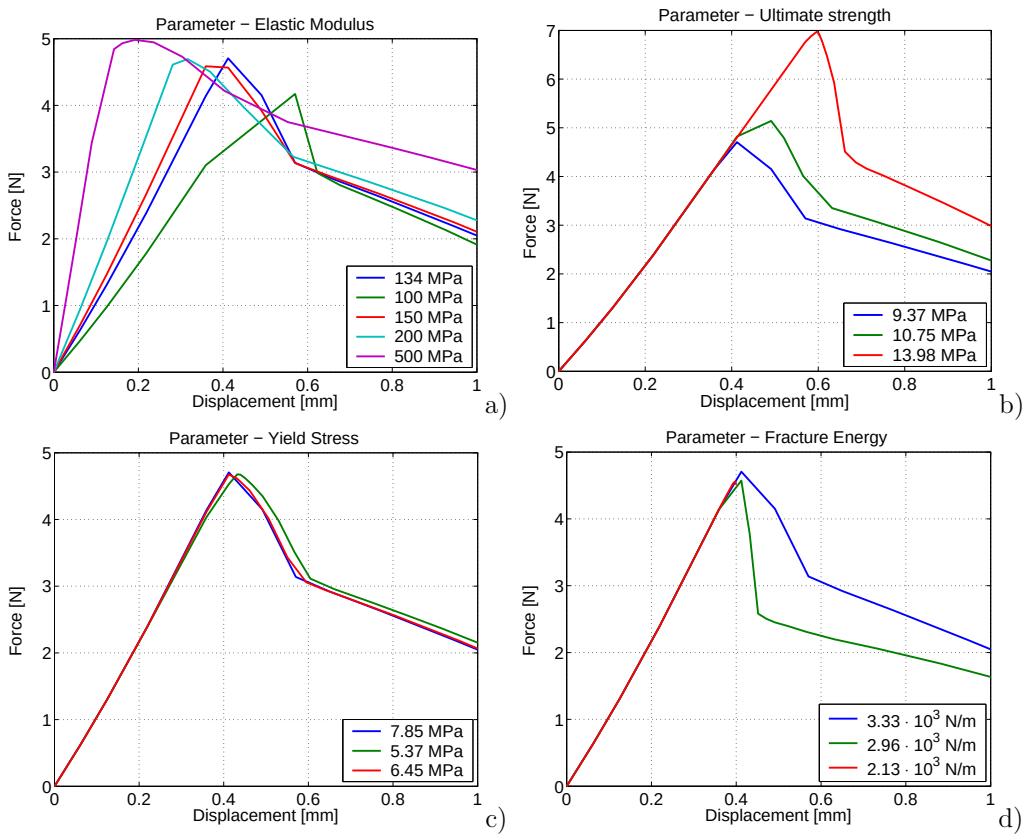

Figure 7.3: *Results of the parameter study (1)*

7.4. Results

The results from the parameter study are presented in forms of force-displacement diagrams. The maximum tear opening force, F_{op}, will be considered as a qualitative parameter result presented in table 7.6.

Parameter	**Value**	F_{op}
(a) Elastic Modulus, E	$100MPa$	$8.34N$
	$134MPa$	$9.42N$
	$150MPa$	$\sim 9.42N$
	$200MPa$	$\sim 9.42N$
	$500MPa$	$9.96N$
(b) Ultimate strength, σ_F	$9.37MPa$	$9.42N$
	$10.75MPa$	$10.28N$
	$13.98MPa$	$13.94N$
(c) Yield stress, σ_y	$7.85MPa$	$\sim 9.42N$
	$5.38MPa$	$\sim 9.42N$
	$6.45MPa$	$\sim 9.42N$
(d) Energy at break, G_F	0.30	$\sim 9.42N$
	0.22	$\sim 9.42N$
(a) Notch	NA	$\sim 9.42N$
	$r = 0.444$	$\sim 8.48N$
	$r = 1.484$	$\sim 7.88N$
(b) Design	w/o Notch & Pull-bridge	$\sim 9.42N$
	Pull-bridge	$\sim 5.40N$
	Pull-bridge & Notch	$\sim 4.54N$

Table 7.6: F_{op} *results*

An increase of the elastic modulus makes the FE-model more stiffer and the tear opening force increases. The results of the parameter study shown in diagram 7.3.a indicates that the initial slope increases and that the zone around the tear opening force, F_{op}, is more rounded. Additionally, the force after the tear opening force descends more rapidly with low values of elastic modulus.

The most important response of the parameter study is the parameter σ_F where an increase of σ_F describes an significant increase of the tear opening force, F_{op}, as shown in diagram 7.3.b.

The modification of the yield stress parameter shows no significant change in the tear opening force as shown in diagram 7.3.c.

The modification of the fracture energy parameter shown in diagram 7.3.d shows to have no influence on the tear opening force, F_{op}. However, the force after the tear opening force descends more rapidly with low values of fracture energy.

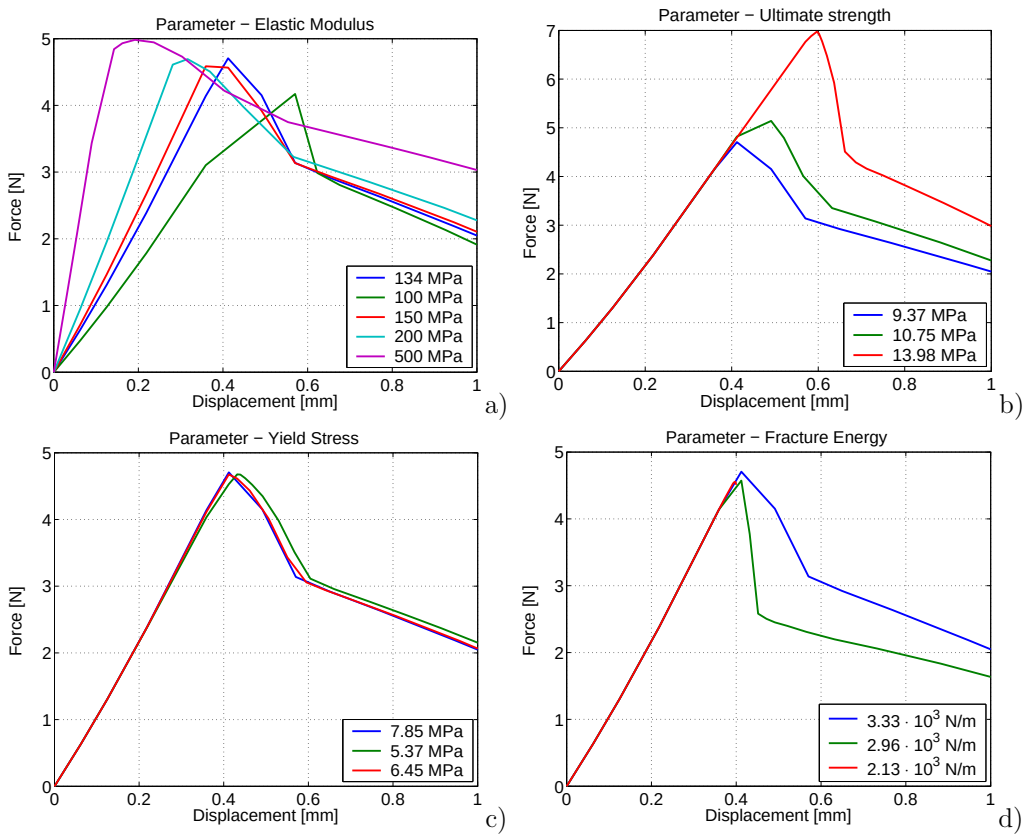

Figure 7.3: *Results of the parameter study (1)*

In diagram 7.4.a the results of the notch modifications in the parameter study are shown. The size of the notch shows to influence the tear opening force where a larger notch results in a smaller tear opening force, denoted *Extended Notch*.

The position of the pull-bridge and the combination of the pull-bridge modification and the notch shows to have important impact on the tear opening force shown in diagram 7.4.b, where an alternative pull-bridge shows to decrease the tear opening force significantly, denoted *Pullbridge*. Additionally, the presence of a notch shows to decrease the tear opening force even more, denoted *Pullbridge & Notch*.

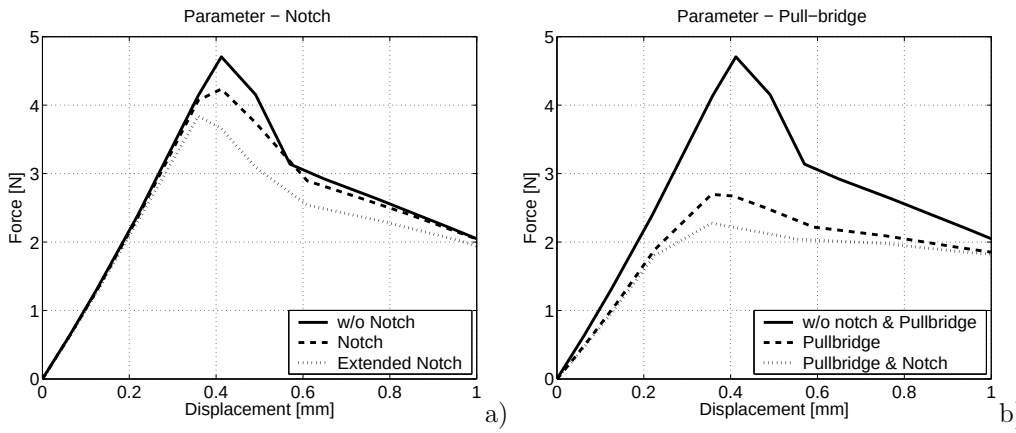

Figure 7.4: *Results of the parameter study (2)*

In addition to the load-displacement curves of the parameter study the development of stress concentrations at the nodes in the fictitious crack plane has been studied. The node with the highest stress concentrations is marked with a larger dot and corresponds at the bold line in the diagram.

In Fig. 7.5.a the node with the highest stress concentration is marked with a larger dot and corresponds at the bold curve in Fig 7.5.b.

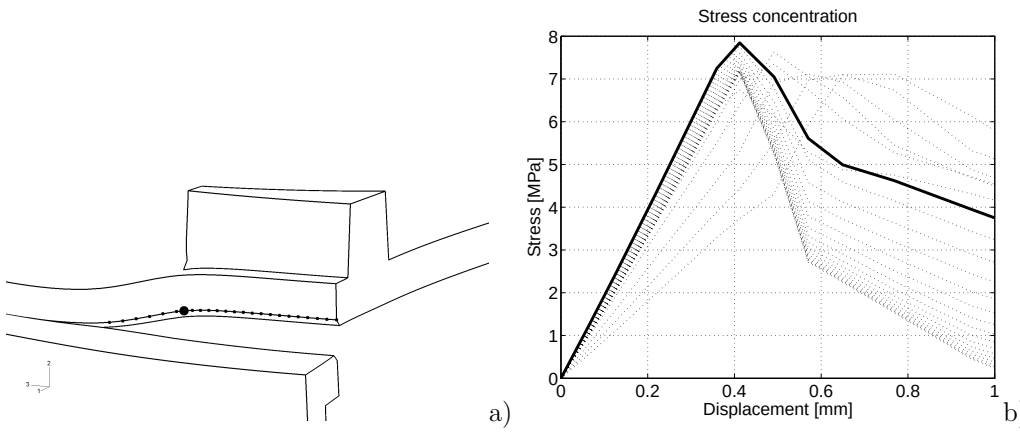

Figure 7.5: *Stress concentration for the FE-model without notch*

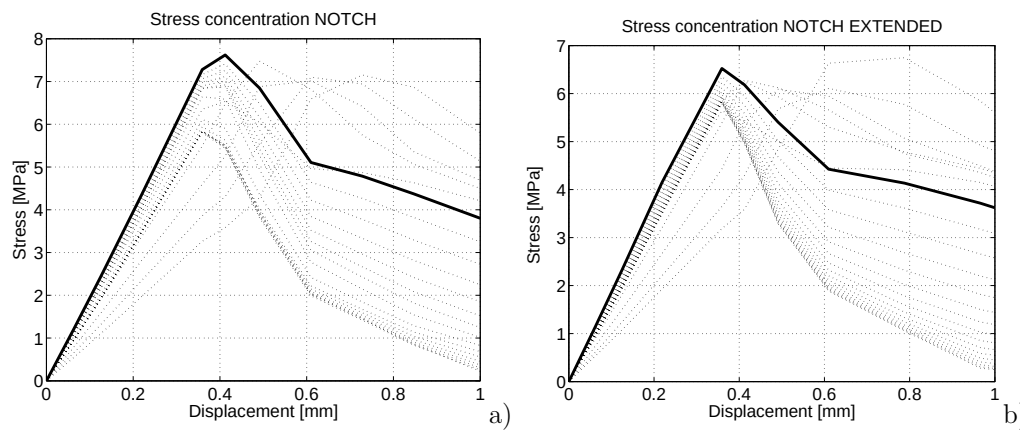

Figure 7.6: *Stress concentrations for the FE-model with a) notch and with b) extended notch*

The results from the notch modifications in the parameter study are shown in Fig. 7.6.a and b. The results of the extended notch is shown in Fig. 7.6.b where smaller stress concentration is encountered than in the case with the standard notch, shown in Fig. 7.6.a.

However, both results correspond at the same node in the fictitious fracture plane as shown in Fig. 7.5.a.

In the case with the combination of pull-bridge and notch the node with the highest stress concentration in the fictitious crack plane is changed, shown in Fig. 7.7.a.

The alternative position of the pull-bridge results in larger stress concentration than in the case with the combination of pull-bridge and notch, shown in Fig. 7.7.b and c. Where both stress concentrations correspond at the same node in the fictitious fracture plane, shown in Fig. 7.7.a.

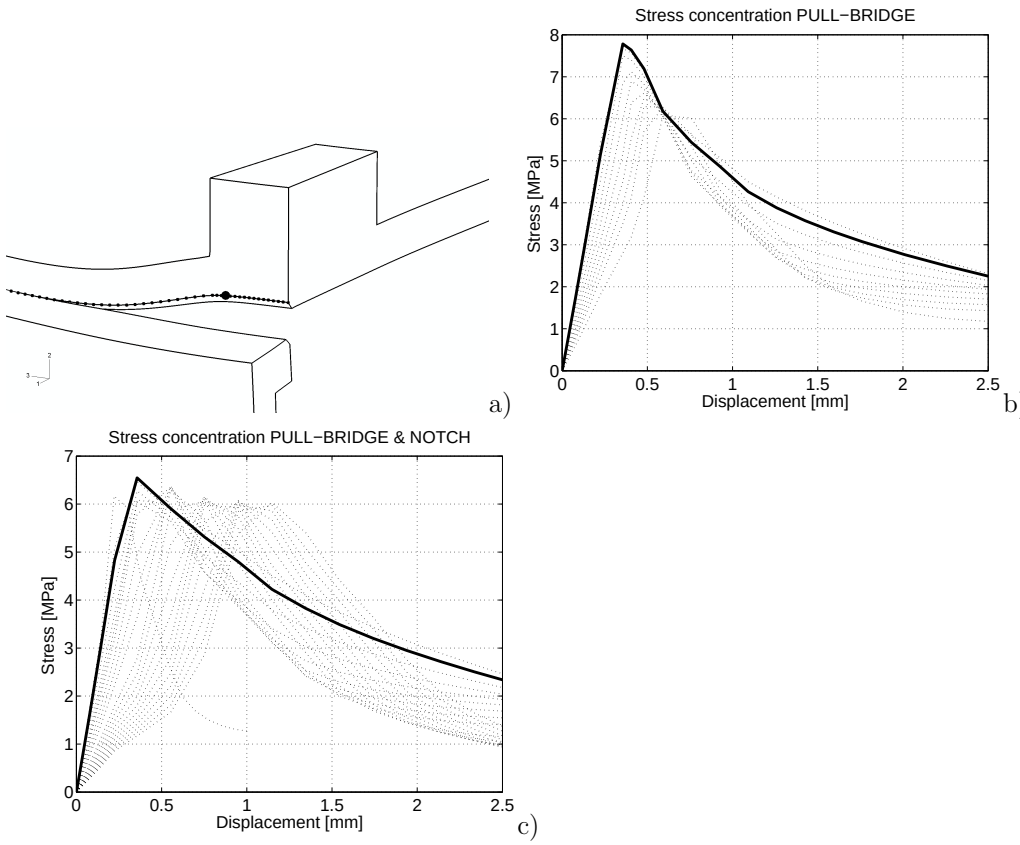

Figure 7.7: *Stress concentrations for the pull-bridge and the combination of pull-bridge and notch.*

Fig. 7.5-7.7 shows that an alternate position of the pull-bridge will change the position of the node with the highest stress concentration to a location more close to the symmetry plane. Notch modifications will thus not affect the position of that node but will influence the stress concentrations at the node.

8. Summary and conclusions

8.1. Summary

The main objectives of this Master's thesis were to establish how the tear opening force reacted with new materials and alternate geometry.

The behavior of the FE-model was based on results from experimental tests of plastic specimens of LDPE and BLEND materials.

The experimental tests were conducted with fairly rapid deformations and consequently the viscoelastic behavior was not brought up.

To simulate fracture of the tear opening in the FE-model a fictitious crack plane was constructed with non-linear springs, representing the deformation softening that was measured in the experimental tests.

8.2. Conclusions

The first steps in this study of the injection molded top included experimental tests of specimens with LDPE, MILK and BLEND material. The tensile tests indicated large deformation of the tensile test specimen and consequently large area changes. It was thus necessary to change the stress strain measures from conventional to true and was consequentially achieved by modelling the experimental tensile test in a FE-environment.

The results from the experimental tests of the top indicated that a peak value always was present with the opening of the package, denoted tear opening force. As the fracture continued the tear opening force descended to a fixed value.

Since the tear opening force was well defined by the experimental tests, the study of the tear opening was focused on this force and how it reacted with new materials and alternate package design.

The tear opening was examined by a numerical parameter study of how material and design parameters influenced the tear opening force, F_{op}.

Material parameters: The ultimate strength showed to have great influence on the tear opening force. Alternate tougher material will raise the ultimate strength and consequently the tear opening force.

Design parameters: A modified geometry of the pull-bride resulted in decreased opening force. The opening force decreased with the presence of a notch as expected.

An increase of ∼100% of the opening force to 63.4N is shown when the BLEND material is used instead of the LDPE material in the tear opening. With the use of notch and modified pull-bridge the opening force can be decreased to 34.2N as shown in Fig. 8.1. These results was achieved by FE-simulation of the top with the BLEND material in combination with numerical parameter study.

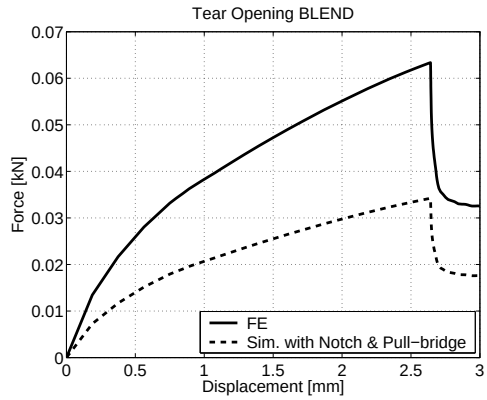

Figure 8.1: *Opening force for the BLEND material*

8.3. Future work

Some suggestions of work within this field that can be done in the future:

- Investigate to which grade the pull-bridge can be modified in order not to interfere with the cap that is later screwed on the packages.
- Assuming that a weak material could cause the package to break during transportation, it would be interesting to investigate materials with increased ultimate strength that would prevent the package to break during transportation. The material should also have sufficiently low ultimate strength to ensure low tear opening force of the package.
- The experiments and FE-analysis has in this study been performed at room temperature, disregarding the fact that the plastic material is temperature dependent. It would thus be of interest to investigate how/if temperature changes affects the thermoplastic material and consequentially the performance of the tear opening.

Bibliography

[1] E.H. Andrews, *Fractures in polymers*, London, England (1968)

[2] G.I. Barenblatt, *The mathematical theory of equilibrium cracks in brittle fractures*, Advances in applied mechanics, Academic press, VII, p.55 (1962).

[3] Z.P. Bažant, Z. Bittnar, M. Jisásek and J. Mazars, *Fracture and damage in quasibrittle structures: Experiment, modelling and computer analysis*, Great Britain (1994), ISBN 0 419 19280 8

[4] A.W. Birley, R.J. Heath, M.J. Scott, *Plastic materials; Properties and applications* , Glasgow, London (1988) ISBN 0-216-92489-8.

[5] Hibbit, Karlsson, Sorensen, *ABAQUS/Keywords V6.1*, USA (2000)

[6] Hibbit, Karlsson, Sorensen, *ABAQUS/Theory Manual V6.1*, USA (2000)

[7] A. Hillerborg, M. Modeer, P.E. Petersson, *Analysis of crack formation and crack growth in concrete by means of fracture mechanics and finite elements*, Cement and concrete research, 6, No. 6 (1976)

[8] Tetra Pak, Homepage: www.tetapak.com